Scientific Research Publishing

International Journal of Astronomy and Astrophysics, 2025, 15(2), 171-196
https://www.scirp.org/journal/ijaa
ISSN Online: 2161-4725
ISSN Print: 2161-4717

A New Open Cluster Census in the Region of Cygnus OB2 with *Gaia* Data

Leonardo G. Paíz[1,2], María S. De Biasi[1,2], Rosa B. Orellana[1,2], Mariela A. Corti[1,2]

[1]Facultad de Ciencias Astronómicas y Geofísicas, UNLP, La Plata, Argentina
[2]Instituto de Astrofísica de La Plata (Centro Científico Tecnológico La Plata, Consejo Nacional de Investigaciones Científicas y Técnicas, Universidad Nacional de La Plata), La Plata, Argentina
Email: lpaiz@fcaglp.unlp.edu.ar

How to cite this paper: Paíz, L.G., De Biasi, M.S., Orellana, R.B. and Corti, M.A. (2025) A New Open Cluster Census in the Region of Cygnus OB2 with *Gaia* Data. *International Journal of Astronomy and Astrophysics*, **15**, 171-196.
https://doi.org/10.4236/ijaa.2025.152013

Received: April 16, 2025
Accepted: June 27, 2025
Published: June 30, 2025

Abstract

We revisit the Cygnus OB2 region to perform a detailed open cluster census taking profit from the high accuracy of *Gaia* DR3 astrometric and photometric data. HDBSCAN clustering algorithm is applied to the five astrometric parameters (α , δ , $\mu_\alpha \cos\delta$, μ_δ , ϖ) in a circular region centred at $(l,b)=(79.8^\circ,+0.8^\circ)$ of radius 1.5˚ up to $G=19.5$ mag and leads us to detect four unnoticed open clusters named RSL-03, RSL-04, RSL-05 and RSL-06, as well as 20 known clusters. The mean proper motion of the open clusters is determined and the members are identified. The coordinates of the centre of the clusters and radii are calculated and their distances are estimated. The analysis of the mean proper motion and the distance of Bica 1, Bica 2, FSR 0236, FSR 0238, FSR 0224, HSC 625, OC-123, OC-128, NGC 6910, RSL-04, RSL-05, and RSL-06 suggests that these open clusters would be related to Cyg OB2 association. This is the first time that Bica 1 and Bica 2 have been identified using the *Gaia* DR3 five astrometric parameters. Besides, the open cluster HSC 630 would be related to the Left over-density found by our working group in a previous paper as an association candidate.

Keywords

Galaxy, Open Clusters and Associations, Astrometry, Early-Type Stars

1. Introduction

The role that open clusters (OCs) play in studying Galactic formation, structure, dynamics and evolution is well known. Since the number of their members can range from a few hundred to a thousand stars forming loose structures, it may be difficult to distinguish this population from field stars. Precise stellar positions

and proper motions are employed in most open cluster identification methods. In the pre Gaia era, the most used catalogs of OCs containing their fundamental parameters and stellar membership are the New Catalogue of Optically Visible Open Clusters and Candidates [1] and The Milky Way Star clusters [2]. In the Gaia era, the *Gaia* Second Data Release (DR2) [3] dramatically transforms OCs studies. The parameters and members of most of the known open clusters reported in pre-Gaia catalogues have been improved [4]-[6] and many of them are found to be no real clusters [4]. Visual inspection of the stellar distributions in the sky and proper motion space [7]-[9], as well as blind searches in the Galactic disc using machine-learning methods [4] [10]-[13], allow the systematic detection of new OCs and upgrade the census.

The latest data set of *Gaia*, *Gaia* DR3 catalogue [14], builds upon the *Gaia* Early Data Release 3 (EDR3) [15] and improves parallax precisions by 30% and proper motion precisions by a factor of 2 with respect to *Gaia* DR2. It has led to the broadening of the OCs census and make new discoveries, such as the studies of Li *et al.* (2022) [16], Hao *et al.* (2022) [17], and Castro-Ginard *et al.* (2022) [18]; the latter refines the census in almost 50% of the known OCs population. Recently, Hunt & Reffert (2023) [19] created a catalogue of clusters using *Gaia* DR3 data down to magnitude $G \sim 20$ which contains 4105 highly reliable clusters, 739 of which are new ones.

The region of Cyg OB2 association, the most massive OB association within 2 kpc distance of the Sun, contains a complex spatial structure along the line of sight with several stellar groupings: Cyg OB2 association, Left and Right over-densities found by Orellana *et al.* (2021) [9] and many open clusters. These OCs have been investigated by Cantat-Gaudin *et al.* (2020) [5], Castro-Ginard *et al.* (2020) [12], Dias *et al.* (2021) [6], Orellana *et al.* (2021) [9], Hao *et al.* (2022) [17] and Hunt & Reffert (2023) [19] (see **Table 1**).

The aim of this work is to perform an elaborate census of the open clusters situated in the Cygnus OB2 region as well as to detect new ones taking profit of the high accuracy of *Gaia* DR3 data up to magnitude $G = 19.5$ mag. For each OC, the astrometric parameters are determined and their members are identified. In addition, the physical parameters such as age and reddening value are investigated.

This paper is organized as follows. Section 2 describes the data used in this work. In Section 3 we describe the procedure employed to detect the OCs located in the Cygnus OB2 region. Results are presented in Section 4. Our conclusions are summarised in Section 5.

2. Data

Gaia is the current astrometry mission of the European Space Agency (ESA), continuing the success of the Hipparcos mission. Its third release of data, *Gaia* DR3 includes the astrometric solution for 1468 million sources, with a limiting magnitude of about $G \sim 21$ and a bright limit of about $G \sim 3$.

Table 1. Position, mean proper motion and parallax of the known OCs determined by different authors.

Open Cluster	α_c	δ_c	$\mu_\alpha \cos\delta_c$	μ_{δ_c}	ϖ_c	Reference
	[deg]	[deg]	[mas/yr]	[mas/yr]	[mas]	
Dolidze 8	306.129	42.300	−2.633 ± 0.190	−5.910 ± 0.195	0.993 ± 0.063	[5]
	306.117	42.299	−2.661 ± 0.191	−6.033 ± 0.253	0.986 ± 0.059	[6]
	306.126	42.290	−2.540 ± 0.216	−6.207 ± 0.232	1.020 ± 0.057	[19]
Roslund 6	307.185	39.798	5.875 ± 0.340	2.155 ± 0.274	2.809 ± 0.076	[5]
	307.128	39.730	5.919 ± 0.344	2.175 ± 0.285	2.816 ± 0.088	[6]
	307.593	40.356	5.950 ± 0.275	2.130 ± 0.231	2.831 ± 0.062	[19]
Cr421	305.829	41.701	−3.651 ± 0.123	−8.334 ± 0.113	0.813 ± 0.048	[5]
	305.837	41.703	−3.651 ± 0.131	−8.336 ± 0.128	0.818 ± 0.062	[6]
	305.817	41.695	−3.640 ± 0.115	−8.372 ± 0.138	0.831 ± 0.054	[19]
NGC 6910	305.797	40.771	−3.415 ± 0.150	−5.359 ± 0.164	0.545 ± 0.052	[5]
	305.789	40.767	−3.431 ± 0.170	−5.373 ± 0.151	0.539 ± 0.054	[6]
	305.802	40.774	−3.296 ± 0.174	−5.423 ± 0.021	0.569 ± 0.031	[19]
UBC 585	306.986	40.558	−2.819 ± 0.056	−5.520 ± 0.063	0.663 ± 0.017	[12]
	307.000	40.548	−2.829 ± 0.048	−5.528 ± 0.053	0.663 ± 0.015	[5]
	306.998	40.542	−2.830 ± 0.070	−5.500 ± 0.070	0.690 ± 0.025	[9]
	306.964	40.555	−2.852 ± 0.076	−5.544 ± 0.123	0.675 ± 0.027	[19]
FSR 0238	308.693	41.417	−2.902 ± 0.177	−4.547 ± 0.127	0.596 ± 0.059	[5]
	308.710	41.476	0.198 ± 0.288	−3.206 ± 0.138	0.736 ± 0.046	[19]
FSR 0236	308.168	41.442	−2.491 ± 0.394	−4.076 ± 0.243	0.522 ± 0.163	[6]
OC-124	306.448	40.911	−3.017 ± 0.223	−4.558 ± 0.440	0.546 ± 0.026	[17]
	306.438	40.924	−3.115 ± 0.073	−4.137 ± 0.064	0.491 ± 0.028	[19]
OC-123	306.321	40.793	−3.005 ± 0.176	−4.828 ± 0.319	0.551 ± 0.026	[17]
	306.356	40.895	−3.047 ± 0.077	−4.733 ± 0.136	0.547 ± 0.025	[19]
OC-128	308.029	40.857	−2.835 ± 0.303	−4.526 ± 0.372	0.580 ± 0.032	[17]
	307.939	40.741	−3.039 ± 0.130	−4.348 ± 0.138	0.574 ± 0.029	[19]
FSR 0224	306.351	40.224	−3.242 ± 0.343	−4.373 ± 0.268	0.566 ± 0.068	[6]
	306.339	40.220	−3.162 ± 0.069	−4.327 ± 0.072	0.574 ± 0.026	[19]
Dolidze 11	306.682	41.372	−1.255 ± 0.109	−4.260 ± 0.184	0.490 ± 0.092	[5]
	306.691	41.376	−1.214 ± 0.194	−4.133 ± 0.201	0.471 ± 0.070	[19]
Bica 2	308.315	41.307	−2.660 ± 0.244	−4.378 ± 0.230	0.555 ± 0.102	[6]
	308.319	41.301	−2.691 ± 0.107	−4.413 ± 0.108	0.576 ± 0.024	[19]
HSC 618	306.745	40.053	−1.997 ± 0.166	−3.963 ± 0.251	1.015 ± 0.040	[19]
HSC 625	308.198	40.838	−2.601 ± 0.085	−4.900 ± 0.098	0.574 ± 0.026	[19]
HSC 626	306.691	41.669	−3.102 ± 0.077	−4.680 ± 0.101	0.535 ± 0.035	[19]
HSC 630	307.710	41.449	−2.007 ± 0.058	−2.918 ± 0.114	0.751 ± 0.033	[19]
FSR 0227	307.250	40.486	−1.838 ± 0.145	−4.584 ± 0.106	0.497 ± 0.037	[19]
HSC 624	307.284	41.264	−2.542 ± 0.122	−3.459 ± 0.365	0.598 ± 0.028	[19]
IRAS-20306+4005	308.059	40.292	−1.811 ± 0.259	−3.997 ± 0.162	1.009 ± 0.098	[19]

The astrometric parameters used in this work are position, parallax, and proper motion, referred to the ICRS at reference epoch J2016.0 [14]. The median uncertainty in parallax and position at the reference epoch J2016.0 is about 0.01 - 0.02 mas for $G<15$ mag, 0.05 mas for $15<G<17$ mag, 0.4 mas for $17<G<20$ mag and 1.0 mas at $G=21$ mag. Referred to the proper motion components, the corresponding uncertainties are 0.02 - 0.03 mas yr^{-1} for $G<15$ mag, 0.07 mas yr^{-1} for $15<G<17$ mag, 0.5 mas yr^{-1} for $17<G<20$ mag and 1.4 mas yr^{-1} at $G=21$ mag [20]. The photometric data employed in this research are the *Gaia* DR3 bands (G, G_{BP}, and G_{RP}) and the near-infrared (NIR) bands (JHK) from the Two Micron All Sky Survey (2MASS) [21]. The photometric errors are those provided by the respective catalogue being $\sigma_G \le 0.01$ mag, $\sigma_{(BP-RP)} \le 0.1$ mag and $\sigma_{(JHK)} \le 0.05$ mag.

A detailed description about the construction of *Gaia* DR3 catalogue can be found in [14]. Data extraction has been performed using the VizieR catalogue database of the Strasbourg astronomical Data Center (CDS).

3. Open Cluster Identification, Membership Determination and Physical Parameters Estimation

3.1. The Sample

We select the stars in a circular region with centre at $(l,b)=(79.8^{\circ},+0.8^{\circ})$ of radius 1.5˚ taking into account the following criteria: 1) The values of the proper motions components are $-5<\mu_\alpha\cos\delta<5$ mas yr^{-1}, $-10<\mu_\delta<0$ mas yr^{-1} (except the case of Roslund 6 whose proper motion values are $-1<\mu_\alpha\cos\delta<10$ mas yr^{-1}, $-1<\mu_\delta<10$ mas yr^{-1}) because a visual inspection of the Vector Point Diagram (VPD) of the region showed low proper motions for the possible OCs candidates. 2) The stars having the Dup value in the catalogue equal to 1 are not selected because they have multiple source identifiers. 3) The parallax values adopted are $\varpi>0.4$ mas. This is based on the range of observed parallaxes in region by Orellana *et al.* (2021) [9]. 4) Stellar parallaxes having fractional error $f=\frac{\sigma_\varpi}{\varpi}>0.20$ are excluded. This restriction reduces the problems in the transformation of parallax to distance. 5) The stars with RUWE parameter ≤ 1.4 [22] are selected because this value is a quality indicator of the astrometric solution. The final sample consists of 23,106 stars with $G\le 19.5$ mag, this cutoff in the magnitude is due to the adopted value of the fractional error.

3.2. Astrometric Analysis

3.2.1. HDBSCAN Algorithm

We apply the HDBSCAN (Hierarchical Density Based Spatial Clustering of Applications with Noise) clustering algorithm [23] to the *Gaia* DR3 astrometric parameters (α, δ, $\mu_\alpha\cos\delta$, μ_δ, ϖ) to detect the clusters and their members in the Cygnus OB2 region. HDBSCAN is an unsupervised learning tool that allows us to identify stellar groups with different density and shape. This algorithm can work with multidimensional data, which must be previously normalized. Normal-

ization allows us to compare different astrometric parameters and make inferences about their distribution. When the entire set of parameters is on the same scale, it is possible to identify and visualize the relationships between them and make meaningful comparisons. In this work, we use Min-Max scaling which transforms the values of each set of parameters between 0 and 1 by

$$x_{scaled} = \frac{x - \min(x)}{\max(x) - \min(x)}, \tag{1}$$

where x is the original value of the astrometric parameter; $\min(x)$ and $\max(x)$ are the minimum and maximum values of the parameter in its dataset, respectively and x_{scaled} is the normalized value of the parameter.

The algorithm requires a metric that calculates the distance between points in the normalized dataset to identify the different densities. The Euclidean metric is the most commonly used [24].

HDBSCAN needs two hyperparameters previously defined to be executed [23]: *minimum number of samples* (mPts) and *minimum cluster size* (mcSize). One of them, mPts, defines the minimum number of neighbouring stars that any star must have to be considered in a grouping. The other hyperparameter, mcSize, is the minimum number of stars required to define a cluster. Different combinations of these hyperparameters give different sizes of clusters. Thus: 1) small *minimum number of samples* and *minimum cluster size* results in many small clusters; 2) small *minimun number of samples* and large *minimun cluster size* results in larger clusters and 3) a large *minimun number of samples* and large *minimun cluster size* results in very large clusters.

Besides, the HDBSCAN algorithm has the disadvantage of identifying false clusters. The identification of real clusters is carried out by adopting the following empirical criteria proposed by Hunt & Reffert (2021) [25]:

a) the dispersion of the total proper motion of their members must satisfy

$$\sqrt{\sigma^2_{\mu_\alpha \cos\delta} + \sigma^2_{\mu_\delta}} \leq \begin{cases} 1\ \text{mas} \cdot \text{yr}^{-1} & \text{if } \varpi \leq 0.67\ \text{mas} \\ 1.49 \cdot \varpi\ \text{mas} \cdot \text{yr}^{-1} & \text{if } \varpi > 0.67\ \text{mas}; \end{cases} \tag{2}$$

b) the radius of the open cluster containing half of its members (r_{50}) must be less than 20 pc;

c) those candidates that have a density compatible with the field stars are discarded. This is implemented by calculating the distance from each star to its ninth nearest neighbour.

In order to determine the optimal values of mPts and mcSize to detect the OCs, and setting mPts and mcSize to the same value as recommended by Campello *et al.* (2013) [23], several runs of HDBSCAN are performed using different combinations of these hyperparameters, both values are in the 5 - 80 range.

Then, for each pair mPts-mcSize we evaluate if the different clusters fulfil a), b) and c) criteria in order to obtain well-characterized OCs.

3.2.2. Stellar Membership Determination and Cluster Parameters

A probable cluster member is found when its HDBSCAN membership probability

is $P \geq 0.5$, following the Bayes minimum error rate decision rule [26]. The number of stars that fulfil this condition is the number of members N_c, and their coordinates guide to compute the cluster radius r_c.

Among the N_c members, we define as the highly probable members N_{hp} those with $P \geq 0.80$. These N_{hp} lead to calculate the coordinates of the cluster centre (α_c, δ_c), the components of the mean proper motion ($\mu_\alpha \cos\delta_c$, μ_{δ_c}), and calculate the mean value of the parallaxes of the members weighed for their squared uncertainty ϖ_c. An estimation of the distance d_{ϖ_c} is calculated by the inverse of ϖ_c, taking into account the general offset of −0.017 mas [20].

3.3. Photometric Analysis

With the goal to know some physical parameters of the clusters found from the proper motion and parallax analysis, we add the study of colour-magnitude diagram (CMD) with *Gaia* photometric data.

Since Cygnus OB2 is one of the major stellar formation region, it is important to distinguish whether the red colour of each star is due to dust present in the line of sight or it is inherent to the star itself. To achieve this, we cross-match the optical *Gaia* data of the stars identified as cluster members with the near-infrared (NIR) photometric data from the 2MASS catalogue (*JHK* bands). For this, we take a maximum angular distance of 1". Then, using the NIR photometric data, we calculate the reddening-free photometric parameter $Q_{NIR} = (J-H) - 1.7 \times (H-K)$ [27] to avoid any confusion arising from the intrinsic degeneracy between reddening and spectral type. We substantiate our star classification by analysing the Q_{NIR} value on the guidelines provided by Borissova *et al.* (2012) [28] and Messineo *et al.* (2012) [29]. Then, $-0.3 < Q_{NIR} < 0.5$ indicates early main sequence stars, $Q_{NIR} < -0.3$ Pre-Main Sequence Stars (PMS) or Young Stellar Objects (YSO) and $0.5 < Q_{NIR}$ late reddening stars.

The extinction value (Av) for clusters is estimated using the new three-dimensional (3D) map of dust reddening, which integrates *Gaia* DR2 parallaxes, stellar photometry data from Pan-STARRS1 and 2MASS, and a hierarchical Bayesian model of dust distribution [30]. The Av value derived from this approach is applied in conjunction with the reddening law: $A_G = 0.83627\,Av$, $A_{BP} = 1.08337\,Av$, and $A_{RP} = 0.63439\,Av$, to fit the appropriate isochrone. When the Av value appears to be inaccurate, we adopt an initial assumption of an Av that closely aligns with the values provided by Wright *et al.* (2015) [31]. Additionally, we consult the APASS[1] catalogue to obtain the V and B photometric data for each star, which are combined with JHK 2MASS bands to estimate the visual extinction for each cluster.

The PARSEC v1.2S isochrones [32] are adjusted to the observed data in the photometric diagram G vs ($G_{BP} - G_{RP}$). To achieve this, we consider the cluster's distance derived from its parallax determination and adopt an initial value of

[1] http://www.aavso.org/apass.

visual absorption as explained previously, which sometimes requires refinement through successive isochrone adjustments. Estimating the age of the open cluster using broadband photometric data and a limited number of stellar members leads to less reliable results. For this reason, we fit multiple isochrones and in all of them we use solar metallicity as a fixed parameter. The true metallicity value of a cluster is determined through the spectral analysis of its individual members. For this reason, we consulted the spectroscopic catalogue by Fu *et al.* (2022) [33], in which the open cluster Collinder 421 is reported to have a metallicity index of [Fe/H] = −0.02 ± 0.04 dex, and the Qin *et al.* (2023) paper [34], where Roslund 6 is given a metallicity index of [Fe/H] = −0.01 ± 0.10 dex. Therefore, as a first approximation, solar-metallicity isochrones could be adopted for all the open clusters studied in the region. In the figures presenting the CMDs for each open cluster, we show the minimum and maximum values of the selected age range with solar metallicity isochrones.

4. Results

4.1. Astrometric Results

The astrometric analysis of the Cyg OB2 region is done following the procedure given in subsections 3.2.1 and 3.2.2. For different values of the hyperparameters (mPts-mcSize), the HDBSCAN algorithm is applied to the sample and several groupings are found. We evaluate if these groupings fulfill the empirical criteria a), b) and c) in order to detect OCs. Therefore, the values of the pair (mPts-mcSize) that well characterize the detected 24 OCs for each final run are given in Table 2.

Table 2. The pair (mPts-mcSize) that well characterize the detected 24 OCs.

OC	mPts	mcSize	OC	mPts	mcSize
Dolidze 8	15	15	Dolidze 11	15	15
IRAS-20306 + 4005	15	15	NGC 6910	15	15
Cr421	15	15	UBC 585	15	15
HSC 630	15	15	HSC 618	15	15
RSL-03	5	5	HSC 625	20	20
RSL-04	10	10	HSC 626	10	10
RSL-05	5	5	FSR 0227	15	15
RSL-06	5	5	OC-123	15	15
FSR 0238	15	15	OC-128	15	15
FSR 0236	15	15	Bica 1	15	15
OC-124	15	15	Bica 2	5	5
FSR 0224	15	15	Roslund 6	30	30

Figure 1 shows the spatial distribution of all clusters identified in the line of sight of Cygnus OB2. Table 3 shows the values of the cluster parameters found and defined in Subsection 3.2.2. A catalogue containing the position (α, δ), the Gaia DR3 identifier, the parallax ϖ and its error σ_{ϖ}, the proper motion components $\mu_{\alpha}\cos\delta$, μ_{δ} and the G magnitude of the members of each cluster will be available online.

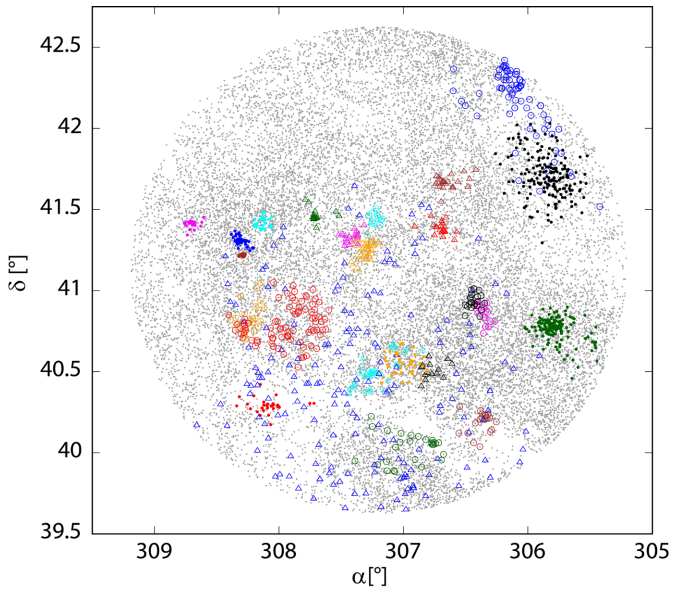

Figure 1. Spatial distribution of the 24 OCs found in the region. Dolidze 8 is drawn in blue circles, Cr421 in black dots, OC-124 in black circles, NGC6910 in green dots, OC-123 in pink circles, FSR 0224 in brown circles, HSC 618 in green circles, UBC 585 in yellow dots, FSR 0227 in turquoise triangles, Roslund 6 in blue triangles, IRAS-20306+4005 in red dots, OC-128 in red circles, HSC 625 in yellow circles, Bica 1 in brown dots, Bica 2 in blue dots, FSR 0238 in pink dots, FSR 0236 in turquoise dots, HSC 630 in green triangles, RSL-03 in turquoise circles, Dolidze 11 in red triangles, RSL-04 in black triangle, RSL-05 in yellow triangle, RSL-06 in pink triangle and HSC 626 in brown triangles.

At the beginning of our investigation, a cross-match of the 24 open clusters detected with those known in the region (see Table 1) indicated that we had found 18 known clusters and six new ones identified as RSL-01, RSL-02, RSL-03, RSL-04, RSL-05 and RSL-06. We detected that the clusters Bica 1, Bica 2, FSR 0238 and FSR 0236, among the known clusters, are located in the core of the Cyg OB2 association.

During the process of this work, a new OC census is published by Hunt & Reffert (2023) [19] using *Gaia* DR3. In their publication, RSL-01 is identified as IRAS-20306+4005 and RSL-02 as HSC 630 (see Table 1 and Table 2). Figure 2 shows the stellar positions, VPD, and parallax histogram for the four new OC members found, IRAS-20306+4005 and HSC 630, while Figure 3 displays the same for Bica 1, Bica 2, FSR 0236 and FSR 0238.

We want to remark that: a) the parallax histogram of IRAS-20306+4005 shows a large range of values. This is because most of the members of this cluster have

magnitudes $17 < G < 19$ mag with parallax uncertainties of 0.4 mas; b) an inspection of the RSL-06 VPD shows a considerable dispersion of its members that has not been possible to justify. However, the stellar position, the parallax histogram and the *Gaia* photometric diagram show it as a cluster. To make a final decision, we will wait for a new series of data from the Gaia mission and we consider RSL-06 as a tentative cluster.

Table 3. Centre coordinates (α_c , δ_c), mean proper motion ($\mu_\alpha \cos\delta_c$, μ_{δ_c}), number of members N_c, number of highly probable members N_{hp} between parentheses, radius r_c, mean parallax ϖ_c and estimated distance d_{ϖ_c} of the detected OCs in the region.

Open Cluster	α_c	δ_c	$\mu_\alpha \cos\delta_c$	μ_{δ_c}	N_c (N_{hp})	r_c	ϖ_c	d_{ϖ_c}
	[°]	[°]	[mas/yr]	[mas/yr]		[arcmin]	[mas]	[pc]
Dolidze 8	306.101	42.252	−2.521 ± 0.207	−6.135 ± 0.210	75 (51)	48.4	1.018 ± 0.039	966 ± 4
IRAS-20306+4005	308.104	40.289	−1.768 ± 0.263	−4.096 ± 0.164	32 (22)	16.8	1.034 ± 0.032	951 ± 6
Cr421	305.821	41.704	−3.641 ± 0.106	−8.359 ± 0.21	175 (119)	25.0	0.822 ± 0.100	1192 ± 2
HSC 630	307.689	41.466	−1.989 ± 0.048	−2.901 ± 0.129	16 (11)	8.1	0.726 ± 0.054	1346 ± 10
RSL-03	307.221	41.436	−2.426 ± 0.103	−3.015 ± 0.035	13 (9)	9.4	0.618 ± 0.012	1575 ± 13
RSL-04	306.780	40.517	−3.126 ± 0.176	−5.179 ± 0.183	15 (10)	7.8	0.558 ± 0.011	1742 ± 24
RSL-05	307.305	41.245	−2.606 ± 0.086	−3.735 ± 0.082	23 (16)	7.9	0.597 ± 0.011	1629 ± 15
RSL-06	307.434	41.323	−3.115 ± 0.190	−4.264 ± 0.159	17 (12)	6.4	0.578 ± 0.016	1682 ± 17
FSR 0238	308.704	41.412	−2.825 ± 0.119	−4.604 ± 0.096	21 (14)	5.0	0.576 ± 0.018	1686 ± 20
FSR 0236	308.133	41.419	−2.334 ± 0.092	−4.161 ± 0.110	26 (17)	4.1	0.585 ± 0.013	1661 ± 12
OC-124	306.437	40.929	−3.117 ± 0.063	−4.124 ± 0.044	22 (15)	6.1	0.500 ± 0.013	1936 ± 21
FSR 0224	306.371	40.198	−3.109 ± 0.097	−4.337 ± 0.087	20 (13)	9.9	0.575 ± 0.017	1688 ± 14
Dolidze 11	306.699	41.381	−1.203 ± 0.120	−4.164 ± 0.109	21 (14)	9.6	0.518 ± 0.033	1868 ± 36
NGC 6910	305.807	40.775	−3.411 ± 0.115	−5.416 ± 0.124	153 (104)	19.1	0.575 ± 0.022	1690 ± 17
UBC585	307.000	40.549	−2.858 ± 0.129	−5.546 ± 0.110	41 (28)	10.9	0.675 ± 0.017	1444 ± 7
HSC 618	306.880	40.025	−2.001 ± 0.178	−4.044 ± 0.180	28 (19)	20.6	1.018 ± 0.024	966 ± 7
HSC 625	308.258	40.792	−2.595 ± 0.077	−4.924 ± 0.089	22 (16)	16.0	0.576 ± 0.022	1686 ± 21
HSC 626	306.661	41.658	−3.096 ± 0.128	−4.678 ± 0.182	23 (16)	16.0	0.530 ± 0.020	1826 ± 18
FSR 0227	307.218	40.488	−1.823 ± 0.157	−4.546 ± 0.137	35 (24)	18.6	0.504 ± 0.017	1919 ± 17
OC-123	306.345	40.840	−3.049 ± 0.058	−4.757 ± 0.112	17 (12)	7.2	0.558 ± 0.011	1740 ± 16
OC-128	307.938	40.798	−3.010 ± 0.127	−4.337 ± 0.107	85 (55)	22.1	0.583 ± 0.014	1682 ± 14
Bica 1	308.296	41.217	−2.775 ± 0.129	−4.507 ± 0.116	22 (15)	1.4	0.578 ± 0.022	1688 ± 13
Bica 2	308.320	41.316	−2.673 ± 0.084	−4.443 ± 0.109	41 (28)	5.4	0.587 ± 0.018	1656 ± 10
Roslund 6*	307.353	40.448	5.999 ± 0.423	2.150 ± 0.374	182	66.7	2.839 ± 0.098	350 ± 1

[*] We compute the mean parameters from all the members found in the region of this study, where the north part of the cluster is occupied.

In the case of Roslund 6, we compute the mean parameters from the N_c members found in the region of this study, where the north part of the cluster is occupied.

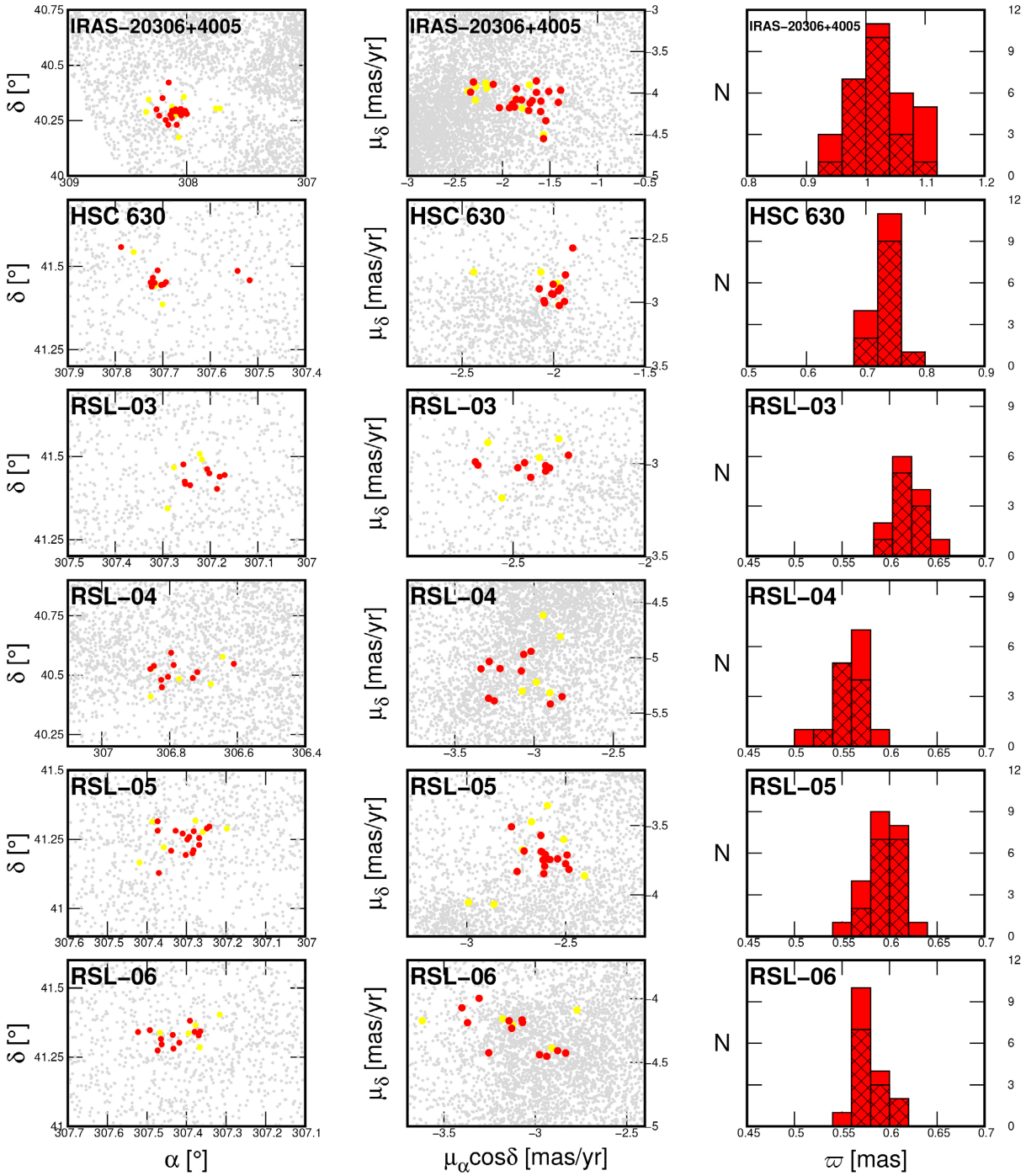

Figure 2. Stellar positions (left column) and VPD (middle column) for the N_c members of the new four OCs detected, IRAS-20306+4005 and HSC 630 (grey circles represent field stars). The N_{hp} members are plotted with red filled circles and the rest of the members with yellow filled circles. The OCs parallax histograms (right column) are shown for the N_c members (red) and for the N_{hp} members (filled with pattern).

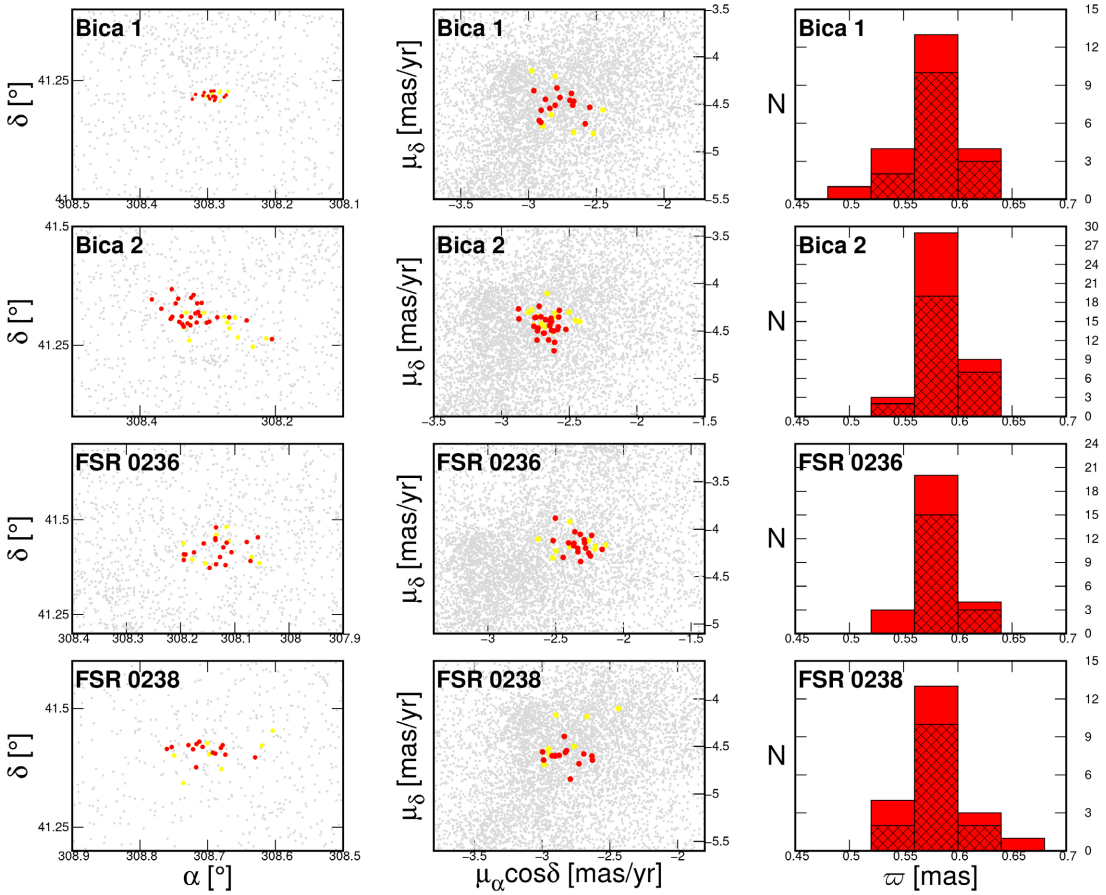

Figure 3. Stellar positions (left column) and VPD (middle column) for the N_c members of Bica 1, Bica 2, FSR 0236 and FSR 0238 located at the core of Cyg OB2 (grey circles represent field stars). The N_{hp} members are plotted with red filled circles and the rest of the members with yellow filled circles. The OCs parallax histograms (right column) are shown for the N_c members (red) and for the N_{hp} members (filled with pattern).

4.1.1. Comparison with Other Works

First, we compare our results given in Table 3 with the ones given in the literature (see Table 1). It can be seen that our values of the centre coordinates, the mean proper motion components and the mean parallax are in good agreement with the literature. The exceptions are the Hunt & Reffert (2023) [19] parameters for FSR 0238 which do not match ours and those obtained by other sources.

Then, as Hunt & Reffert (2023) [19] identify the OCs in the region that have been previously studied using *Gaia* DR2 data, we compare our lists of members with theirs. This comparison distinguishes between common members—stars identified in both datasets—and non-common members, which are exclusive to either our study or theirs. (see Figure 4). We find differences in the number of members, although the catalogue used (*Gaia* DR3) and the method (HDBSCAN algorithm) are the same. Table 4 shows the low percentage of members in common.

We notice that their results contain very faint members, for which parallax uncertainty may distort the spatial distributions in transforming parallax to distance

[35] [36]. To check if this happens, for each OC we examine the histogram of the geometric distance (r_{geo}) of both lists of members using the data from Bailer-Jones *et al.* (2021) [37].

Table 4. Hunt & Reffert (2023) [19] members in common with ours.

Open Cluster	In Common	Open Cluster	In Common
Dolidze 8	59%	Cr421	46%
NGC 6910	53%	UBC 585	67%
OC-124	45%	OC-123	38%
OC-128	51%	FSR 0224	64%
Dolidze 11	19%	Bica 2	33%
HSC 618	61%	HSC 625	53%
HSC 626	61%	HSC 630	68%
FSR 0227	55%	IRAS-20306+4005	43%

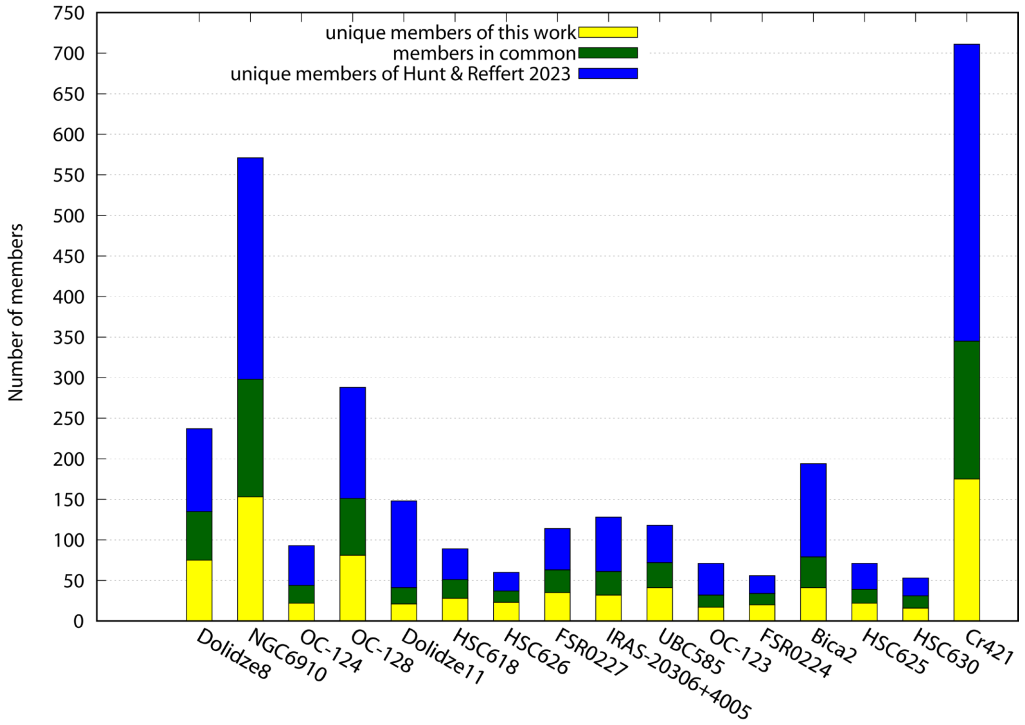

Figure 4. Bar diagram comparing the number of members for each open cluster between our work and that of Hunt & Reffert (2023) [19]. The names of the clusters are displayed along the X-axis, while the Y-axis represents the total number of members. The bars are grouped to distinguish between members identified exclusively in our study (yellow), members identified exclusively in Hunt & Reffert's catalogue (blue), and common members found in both lists of members (green).

As an example, **Figure 5** shows the comparison of results from this study and those from [19] for Dolidze 8. **Figure 5b** plots the results for Dolidze 8 where the histogram of our members shows a Gaussian distribution and the one of Hunt & Reffert (2023) [19] members is skewed to the right, indicating false positives and

a distance range between 800 and 3300 pc.

To explain the presence of these false positives, the uncertainties in the parallaxes of the members are plotted against r_{geo} in **Figure 5c**. It can be seen that the Hunt & Reffert (2023) [19] members with greater parallax uncertainty produce the skewness that distorts their spatial distribution in **Figure 5b**.

On the contrary, **Figure 5b** and **Figure 5c** do not show this distortion for our members. This is due to the adoption of stellar parallaxes with fractional error $f = \frac{\sigma_{\varpi}}{\varpi} \leq 0.20$ (criterion iv) in our sample. For this reason our members have smaller parallax uncertainties, as seen in **Figure 5c**.

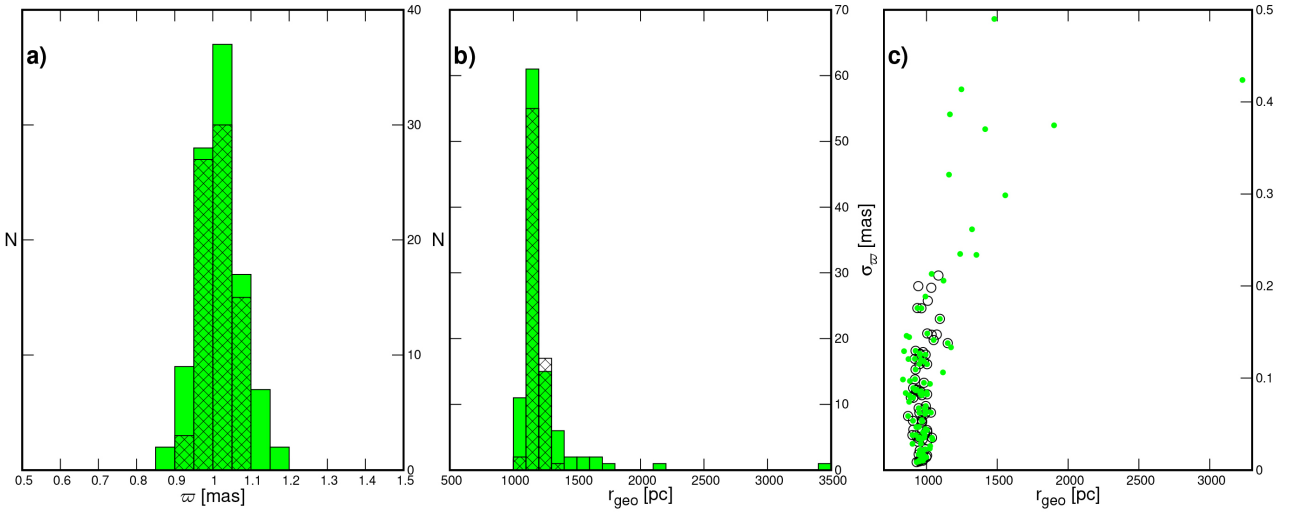

Figure 5. Results for the open cluster Dolidze 8. a) parallax histograms for [19] (green) and this work (filled with pattern). b) geometric distance histograms r_{geo} obtained from [37], for [19] (green) and this work (filled with pattern). c) uncertainty in parallax σ_{ϖ} against r_{geo} for members from [19] (green filled circles) and this work (open black circles).

Table 5. Mean proper motion and parallax of the stellar over-densities determined by Orellana *et al.* (2021) [9].

Association	$\mu_{\alpha}\cos\delta_c$	μ_{δ_c}	d_c
	[mas/yr]	[mas/yr]	[pc]
Cyg OB2	−2.71 ± 0.02	−4.24 ± 0.02	1669 ± 6
Right	0.04 ± 0.02	−3.33 ± 0.02	1281 ± 5
Left	−2.09 ± 0.02	−3.02 ± 0.02	1284 ± 5

We also notice that the members of Bica 2 identified by Hunt & Reffert (2023) [19] are located in the place where OC census carried out prior to Gaia era identifies Bica 1 and Bica 2 separately [38]. Our analysis finds both clusters. Besides, it is not possible to detect HSC 624 in our work, even several runs of HDBSCAN have been done using different values of mPts and mcSize; instead we detect two new OCs named RSL-03 and RSL-05. The former corresponds to the northeast

part of HSC 624, and the latter to the southwest part of it.

4.1.2. Spatial Structure along the Line of Sight of the 24 Open Clusters

We analyse the spatial structure along the line of sight of the selected circular area. In **Figure 6**, we plot the mean proper motion components of the open clusters detected in this study with dots (except Roslund 6, Cr 421 and Dolidze 8 whose values are out of the range of the axes of the figure). The different colours represent the scale of the estimated distances.

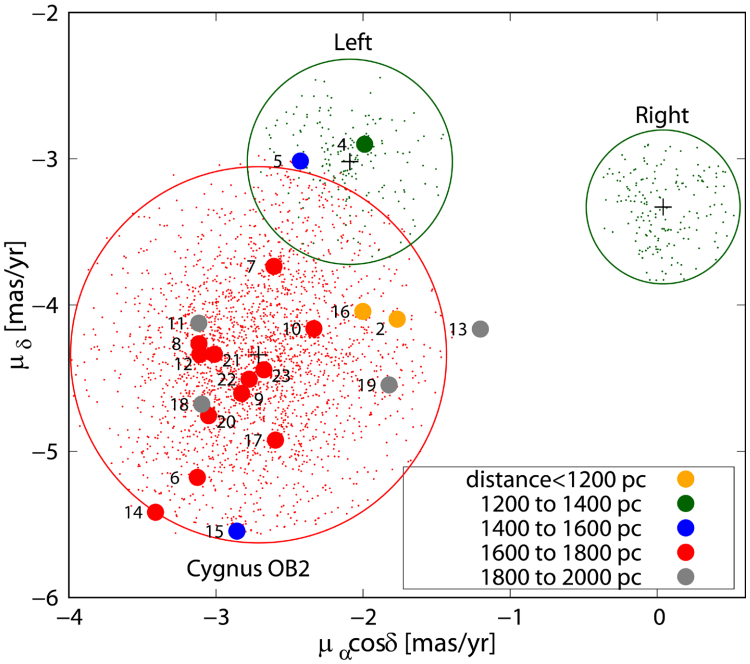

Figure 6. Vector point diagram (VPD) of the region except Dolidze 8, Cr421 and Roslund 6. OCs mean proper motion are plotted with filled circles, and the members of Cyg OB2 association, Left and Right stellar groups are plotted with dots.

Also, we plot the members of the Cyg OB2 association, Left and Right over-densities found by Orellana *et al.* (2021) [9] with the colour according to their distance. The red circle contains the proper motion values of the members of Cyg OB2, and the green ones contain the proper motion values of the members of the Left and Right over-densities. The mean proper motion of Cyg OB2 association, Left and Right over-densities are plotted with crosses (see **Table 5**).

It can be seen that the estimated distance of several clusters is between 1600 and 1800pc, similar to the distance of Cyg OB2 and their mean proper motions lie inside the red circle. These clusters and their numbers in **Figure 6** are FSR 0224 (no. 12), FSR 0236 (no. 10), FSR 0238 (no. 9), RSL-04 (no. 6), RSL-05 (no. 7), RSL-06 (no. 8), HSC 625 (no. 17), OC-123 (no. 20), OC-128 (no. 21), NGC 6910 (no. 14), Bica 1 (no. 22) and Bica 2 (no. 23). This suggests that these OCs would be connected to Cyg OB2 association.

We also notice that the estimated distance of HSC 630 (no. 4) is similar to the

distance of the Left over-density, and that the mean proper motion of the OC lies inside the green circle. Then, HSC 630 would be connected to the Left over-density.

In the case of the Right over-density, there is no OC in the region having similar mean proper motion and estimated distance.

4.2. Photometric Results

An important result of the photometric analysis is the age of an OC. Its determination is a serious problem related to the contamination by field stars, unresolved binarity of the cluster stars and variable interstellar reddening.

In order to reduce the first and second effects on the astrometric membership determination, we impose restrictions on the sample (Subsection 3.1) that allow the photometric analysis to be more reliable.

The Gaia DR3 catalogue allows us to reach fainter magnitudes which provide many more cluster members. However, we must be careful with the contamination by field stars that can be produced by the astrometric parameter uncertainties. The effect of parallax uncertainty has been reduced by considering $\frac{\sigma_{\varpi}}{\varpi} \leq 0.20$ in our sample (criterion iv) and demonstrated in 0.0.3. The rest of the possible field stars are eliminated by defining the highly probable members N_{hp} as those with $P \geq 0.80$ (section 3.2.2).

Regarding stellar binarity, Belokurov *et al.* (2020) 39] demonstrate that a high RUWE value is an effective indicator of it, as well as Lindegren (2022) [40] remarks that RUWE is its main indicator. Following Castro-Ginard *et al.* (2024) [41], we can say that our sample is free of its contamination by considering a RUWE ≤ 1.4, which is the criterion v) adopted in Subsection 3.1. Therefore, the astrometric members obtained in 1 are ready for a reliable photometric analysis.

Interstellar reddening is another important factor to address when determining the age of open clusters. In a region with variable interstellar reddening, to know the extinction value becomes a challenging task. The correct fit of the isochrone to the observations is directly dependent on the value of Av. In this work, this value is estimated using the new three-dimensional (3D) dust reddening map and is then applied in conjunction with the *Gaia* photometric reddening law, as explained in Subsection 3.3.

We present the evaluation of the *Gaia* DR3 photometric diagram of the four RSL new open clusters identified, IRAS-20306+4005 and HSC 630 plotted in **Figure 7**, and those in the core of Cyg OB2 association, plotted in **Figure 8**. Red filled circles correspond to the N_{hp} members, and the yellow circles indicate the rest of the members. The isochrone is fitted based on the red filled circles. In all the CMD figures, the isochrone presented in black corresponds to the most probable age estimated for each OC, while the isochrones in yellow and green, as observed, also appear to fit the stellar member observations. Then, an estimation of the error in the age is the difference between the ages of yellow and black isochrones and between the ages of green and black ones. The isochrones in light blue and blue

represent the age range investigated.

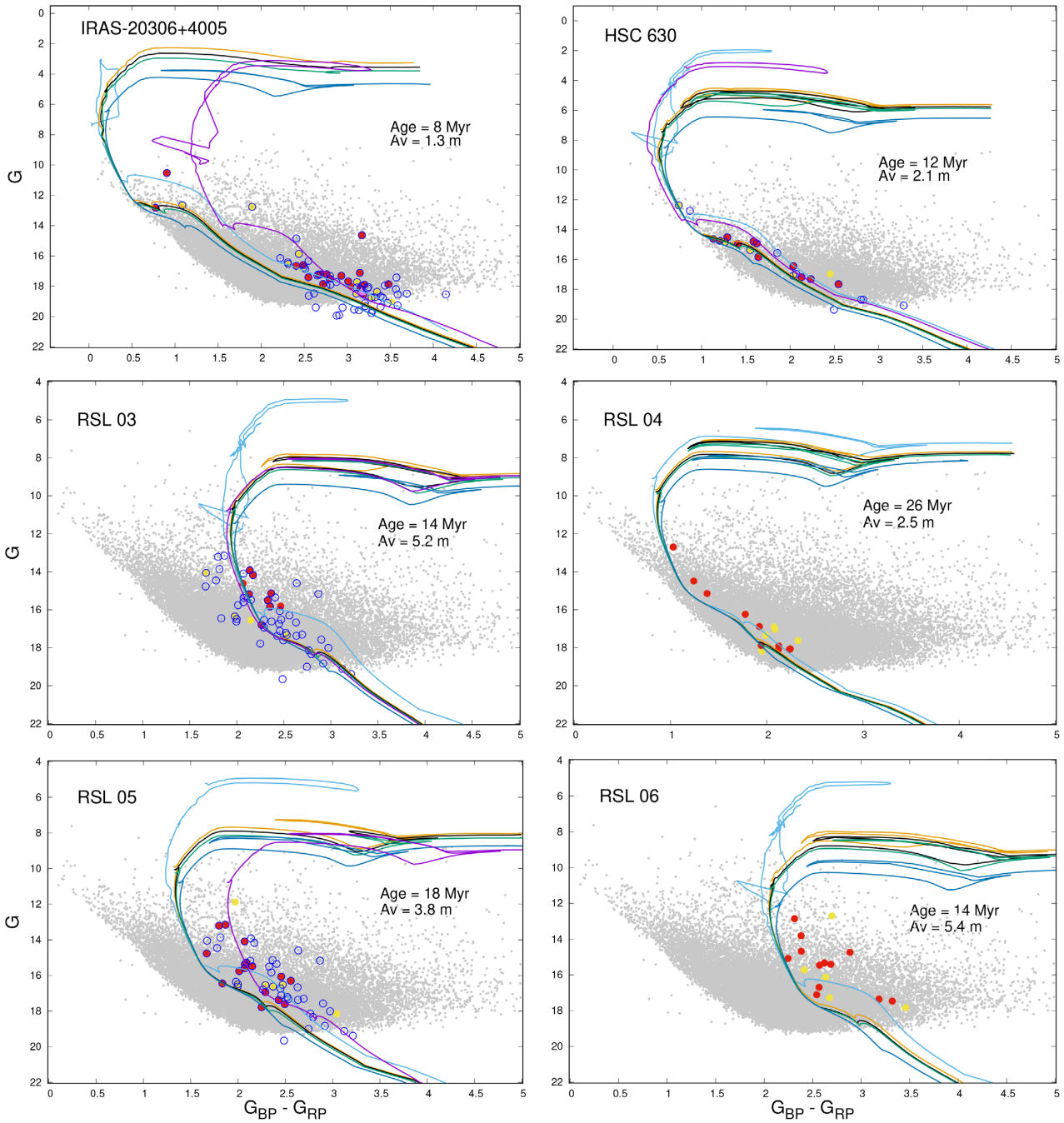

Figure 7. *Gaia* photometric diagram for the probable members of the four RSL new open clusters, IRAS-20306+4005 and HSC 630. Light gray dots correspond to the field population. Red filled circles are the N_{hp} members of each cluster obtained in this paper while the yellow ones are the rest of the members. Open blue circles are the members found by Hunt & Reffert (2023) [19]. Magenta triangle in the IRAS-20306+4005 CMD represents the star with IR excess identified as BY DRA Variable by Chen *et al.* (2020) [43]. The black isochrone corresponds to the most probable age estimated for each OC. The magenta isochrone represents the evolutionary model of stars reported by Hunt & Reffert (2023) [19].

In these figures, Hunt & Reffert (2023) [19] members are plotted with open blue

circles. They are not considered to fit ours isochrones because they may be contaminated by false positives, as shown in Subsection 4.1.1. The magenta curve is the isochrone achieved with the photometric parameters proposed for each open cluster by Hunt & Reffert (2023) [19].

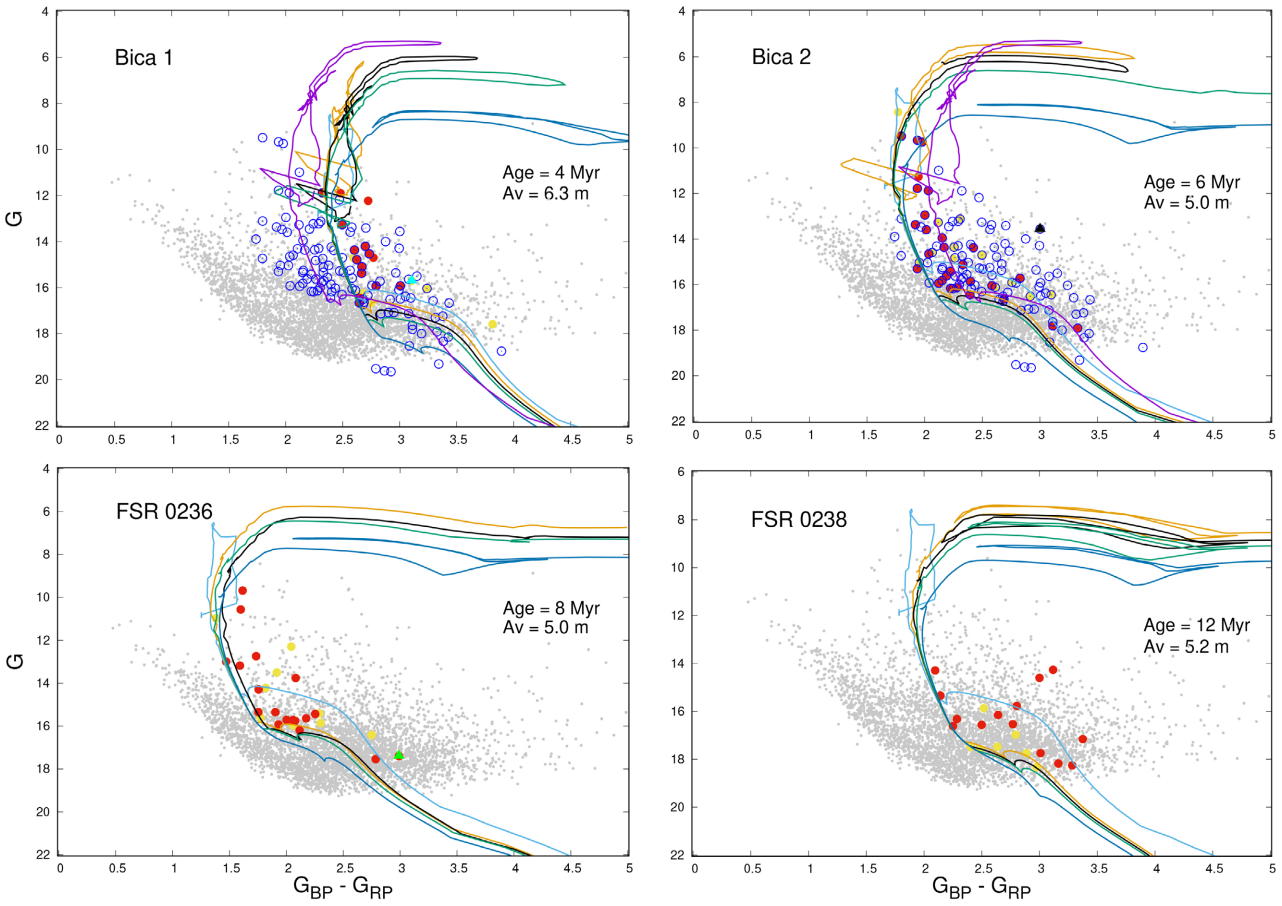

Figure 8. Gaia photometric diagram for the probable members of the four known open clusters in the core of CygOB2. Symbols as in **Figure 4**. Cyan and green triangles represent stars with IR excess identified as YSO by Kuhn *et al.* (2021) [44] and X-ray source as [48], respectively. Black triangle is the emission-line star identified as Schulte 64 by Bhattacharyya *et al.* (2021) [46]. The black isochrone corresponds to the most probable age estimated for each OC. The magenta isochrone represents the evolutionary model of stars reported by Hunt & Reffert (2023) [19].

4.2.1. New OCs

- RSL-01 ≡ IRAS-20306+4005

This cluster, located at less than 1 kpc in the southern edge of the study region, in the line of sight of the Cygnus-X DR 15 Region [42], is plotted in **Figure 1** with red dots. The isochrone for the *Gaia* DR3 catalogue data of the 22 N_{hp} members (upper left in **Figure 7**), is fitted using a visual absorption value of, $Av = 1.3^{+0.02}_{-0.03}$ mag, as determined for this Galactic region in the 3D map. The uncertainties in the Av value correspond to those provided by the map. To estimate the age of this cluster, we fit isochrones within an age range of 2 to 15 Myr, ultimately determining an age of 8 ± 1 Myr. Most of the 32 possible members are likely to be late

spectral types, with only a few exhibiting early spectral types (B and A).

One of its members, the *Gaia* DR3 2064713443456205696 star, $(\alpha,\delta)=(308.0477,40.3021)$ has a reddening-free photometric parameter $Q_{NIR}=-1.17\pm0.13$, and according to what we stated in Section 3.3, this Q_{NIR} value would indicate that this could be a PMS or an YSO star. Additional information available regarding this star indicated in **Figure 7** with a magenta triangle is that Chen *et al.* (2020) [43] classify it as a probable BY Draconis Variable star and they are of K-M type, similar to the spectral type that we can estimate with our best-fitting isochrone. Besides, we notice that all members of Hunt & Reffert (2023) [19] that are below the isochrone determined by us have large uncertainties in the parallax. Their distance histogram shows that 6 of them may be false positives, according to the analysis performed in 4.1.1. The magenta isochrone represents the evolutionary model of stars formed 4.8 Myr ago with solar metallicity, located at a distance of 936 pc and subject to a visual extinction of 3.7 mag, as determined from the 50th percentile results published by Hunt & Reffert (2023) [19].

• RSL-02 ≡ HSC 630

HSC 630 is an OC located near the center of the examined region, at an estimated distance of 1346 pc from the Sun, plotted with green triangles in **Figure 1**. The best-fitting isochrone for its 11 N_{hp} members is obtained with the visual absorption value, $Av=2.1^{+0.08}_{-0.05}$ mag, derived from the 3D map. By studying this region employing images from the Digital Sky Server (DSS), it is evident that the initial dust has already been swept away, which would be consistent with a visual absorption value of only two magnitudes. The age of this OC is investigated within the range of 4 to 22 Myr, and the most probable formation age is 12 ± 1 Myr. The *Gaia* DR3 2068009749251662336 star with $G=12.38$ mag and $(G_{BP}-G_{RP})=0.74$ mag would be the earliest, probably a late B spectral type star whose age corresponds very well with the cluster age. The rest of the members are likely of spectral types A, F, and G. The magenta isochrone represents the 50th percentile results by Hunt & Reffert (2023) [19] with $Av=1.9$ mag, an age of 6 Myr and a distance of 1294 pc.

• RSL-03

This cluster, located near the centre of the study region, at an estimated distance of 1575 pc from the Sun, is plotted in **Figure 1** with turquoise circles. From the 9 N_{hp} members of RSL- 03, the best-fitting isochrone for the *Gaia* DR3 catalogue is obtained with a visual absorption of $Av=5.2^{+0.04}_{-0.14}$ mag, found with these errors in the 3D map. The age of this OC is investigated within the range of 4 to 22 Myr, with an estimated formation age of 14 ± 1 Myr. The spectral type of these stars would be between B and F0. Although the open cluster HSC 624 determined by Hunt & Reffert (2023) [19] has not been detected (see subsection 4.1), for comparison, we have included their isochrone in **Figure 7** because its northeast part coincides with our RSL-03. The physical parameters of HSC 624 determined by

Hunt & Reffert (2023) [19] at the 50th percentile for the members of this cluster are similar to ours, with a distance of 1.6 kpc, an age of 15 Myr, and $Av = 5.1$ mag.

• RSL-04

This cluster is located in the southern right edge of the study region, at an estimated distance of 1742 pc from the Sun, and is plotted in **Figure 1** with a black triangle. The best-fitting isochrone for the 10 N_{hp} members is obtained with a visual extinction of $Av = 2.5^{+0.05}_{-0.03}$ mag, as reported for this Galactic region in the 3D map. The age of the cluster is investigated within the range of 16 to 40 Myr, resulting in 26 ± 2 Myr with A-type and late spectral-type stars. Based on this age, the cluster is among the older open clusters in the Cyg OB2 region.

• RSL-05

RSL-05 is an OC located near the centre of the examined region, at an estimated distance of 1629 pc from the Sun, plotted with yellow triangles in **Figure 1**. The 16 N_{hp} members of RSL-05 are used to obtain the best-fitting isochrone which suggests a visual absorption of $Av = 3.8$ mag and an age of 18 ± 2 Myr. Based on this result, this open cluster would be another member of the older groups of open clusters in the Cyg OB2 region. Some stars are likely to belong to spectral types F and G, while the majority are earlier-type stars, specifically B and A. For this open cluster, the visual extinction value obtained in the Galactic region using the 3D map is $Av = 4.6^{+0.08}_{-0.13}$ mag, so it differs by approximately 1 magnitude from our result. This discrepancy is likely due to the high concentration of interstellar material in the region, along with the fact that the 3D map was generated using data from the *Gaia* DR2 catalogue, which has an inherent 30% uncertainty in parallax measurements compared to the *Gaia* DR3 catalogue. It is evident that the [19] isochrone shown in magenta color exhibits different visual extinction and age, with $Av = 5.1$ mag and age of 15 Myr. This open cluster should be reanalyzed using the data provided by the upcoming *Gaia* DR4 catalogue, which is expected to yield more precise and, therefore, more reliable results. Although HSC 624 has not been detected, in **Figure 4** we include its [19] isochrone as in the study of RSL-03 because its southwest part coincides with our RSL-05.

• RSL-06

The OC RSL-06 is located near the center of the study region, at an estimated distance of 1682 pc from the Sun, plotted with pink triangles in **Figure 1**. RSL 06 contains 12 N_{hp} members and the best-fitting isochrone for these stars is obtained with a visual absorption of $Av = 5.4^{+0.10}_{-0.01}$ mag, found with these errors in the 3D map. The age is investigated within the range of 4 to 30 Myr, with an estimated formation age of 14 ± 1 Myr. These stars would be from B to A9 spectral type. It is important to note that one of the results obtained from the analysis of these six open clusters is that RSL- 03, RSL- 05, and RSL- 06 are located very close to each other, as shown in Figure 0.0.2. They are the clusters for which the highest values of Av are estimated, ranging between 3.8 and 5.4 magnitudes.

4.2.2. Core of Cyg OB2

• Bica 1 and Bica 2

Bica *et al.* (2003) [47] detected Bica 1 and Bica 2 by visual inspection while examining the structure of the association Cyg OB2 with DSS images, both objects are located within the core radius of the association and seem to form a physical pair in the association core. Maíz Apellániz *et al.* (2020) [48] noticed that they are hard to distinguish in proper motion even if they are seen as density concentrations in the plane of the sky. The proper motions in the right ascension of two clusters are very similar while those in declination differ very little.

This work identifies Bica 1 and Bica 2 using the HDBSCAN algorithm, which detects these two objects separately. They are then confirmed as clusters by fulfilling the three criteria outlined in 3.2.1. Proper motion and parallax values suggest that Cygnus OB2 association and each of these clusters are co-moving (see **Figure 6**). The distance measured for both clusters by Maíz Apellániz *et al.* (2020) [48] is ~1.7 kpc, in accordance to our results in **Table 3**. Bica 1 has 15 N_{hp} members. The lack of evolved stars makes it impossible to determine the position of the turn-off point, thus complicating the selection of the correct isochrone. The best-fitting isochrone is found by studying an age range of 2 to 10 Myr. The 4 ± 1 Myr isochrone, with a visual extinction of $Av = 6.3^{+0.07}_{-0.07}$ magnitudes, provides the best fit. It is a very young cluster of stellar members with early spectral types. The *Gaia* DR3 2067782111687592704 star located at $(\alpha, \delta) = (308.2830^{\circ}, 41.2241^{\circ})$ with $Q_{NIR} = -0.52 \pm 0.08$, indicated with cyan triangle symbol on **Figure 8**, represents the YSO by Kuhn *et al.* (2021) [44]. Bica 2 is older than Bica 1 but contains a greater number of probable stellar members with 28 N_{hp} members. It also lacks evolved stars, and the best isochrone fit is found by studying an age range of 2 to 15 Myr with visual absorption, $Av = 5^{+0.06}_{-0.06}$ mag. The estimated formation age for Bica 2 is 6 ± 1 Myr. All these stars have early spectral types. The *Gaia* DR3 2067783559095152768 star located at $(\alpha, \delta) = (308.3271^{\circ}, 41.2597^{\circ})$ and with $Q_{NIR} = -0.18 \pm 0.071$, is a Be star identified as Schulte 64 with Spectral type B1 V [46]. This star is indicated by a black triangle symbol in **Figure 8**. The visual extinction values for Bica 1 and Bica 2, along with their associated errors, are the values assigned to this Galactic region in the 3D map. The magenta isochrone represents the evolutionary model of stars reported by Hunt & Reffert (2023) [19] for Bica 1 and Bica 2, as the authors consider the members of both clusters to be part of a single open cluster. This isochrone corresponds to a stellar cluster located at a distance of 1.6 kpc, formed 3.5 Myr ago, with a visual extinction of 5.6 mag. The age difference shows that both clusters formed at different times.

• FSR 0238

The OC FSR 0238 is located east of the centre of the studied region, at an estimated distance of 1686 pc from the Sun, and is plotted with pink dots in **Figure 1**. The best-fitting isochrone for these stars suggests a probable visual absorption of $Av = 5.2$ mag, which differs by one magnitude from the value obtained for the Galactic region using the 3D map ($Av = 6.2^{+0.06}_{-0.02}$ mag). This discrepancy warrants further investigation with the upcoming *Gaia* DR4. The age is studied in the

range of 2 to 24 Myr, and according to our best-fitting isochrone for the 14 N_{hp} members, the age of this open cluster would be 12 ± 2 Myr. This result aligns well with the possible age of the earliest star, *Gaia* DR3 2067870386152902656, with a spectral type of B V. Although we do not know the exact spectral type of the other members, we can reasonably conclude that they are likely B and A type stars.

• FSR 0236

It is an open cluster close to the core of the Cyg OB2 association at a distance of 1661 pc to the Sun, and is plotted with turquoise dots in **Figure 1**. The best-fitting isochrone for the 17 N_{hp} members suggests that the visual absorption, $Av = 5.0^{+0.08}_{-0.04}$ mag, with the associated errors from the 3D map, represents the interstellar reddening in the region. This Av value is similar to those obtained for Bica 2, and FSR 0238 clusters, which are located in the same region of the Galaxy. The age is study in the range of 2 to 15 Myr and according to our best-fitting isochrone, the age of this open cluster would be 8 ± 1 Myr. The *Gaia* DR3 2067834514587217536 star located at $(\alpha,\delta)=(308.1170^{\circ},41.3803^{\circ})$ and with $Q_{NIR}=-3.05\pm0.2$, is represented by a green triangle symbol in **Figure 8**. This star is one of those investigated by Rauw (2011) [45] during the multi-epoch XMM-Newton campaign on the core of the massive Cyg OB2 association, where it is categorized as an X-ray fainter OB star, but not analyzed in detail, with a possible spectral type of O7 V. Our analysis using the PARSEC isochrone suggests that it is likely a late B spectral type and the rest of the members are also likely to be of spectral type B.

5. Conclusions

The latest version of *Gaia* catalogue, *Gaia* DR3, which has considerably improved proper motions and stellar parallaxes with respect to *Gaia* DR2, allows us to have a better understanding of the objects lying in the direction of the Cyg OB2 association. This region is complex due to the fact that the spatial structure along the line of sight shows several stellar groupings such as the Cyg OB2 association, the Left and Right over-densities found by Orellana *et al.* (2021) [9] and open clusters.

Using the five astrometric parameters of the catalogue *Gaia* DR3 (α, δ, $\mu_\alpha\cos\delta$, μ_δ, ϖ), the HDBSCAN clustering algorithm allows us to detect 20 known OCs (IRAS-20306+4005, Dolidze 8, Roslund 6, Cr421, NGC 6910, UBC 585, FSR 0238, OC-124, OC-123, OC-128, FSR 0224, Dolidze 11, Bica 1, Bica 2, HSC 618, HSC 625, HSC 626, HSC 630, FSR 0236 and FSR 0227) and four unnoticed ones named as RSL-03, RSL-04, RSL-05 and RSL-06 in a circular region centred at $(l,b)=(79.8^{\circ},+0.8^{\circ})$ of radius 1.5˚ up to $G=19.5$ mag. For all these clusters, we calculate the coordinates of the cluster centre, the mean proper motion, and the mean parallax and estimate the distance. Our values are consistent with those reported in the literature. This is the first time that Bica 1 and Bica 2 have been identified using the Gaia DR3 five astrometric parameters, and their parameters have improved with high precision. In addition, the members of FSR 0236 and FSR 0238 are identified with *Gaia* DR3 data for the first time and the

parameters of the clusters are determined. The analysis of the mean proper motion and distance for FSR 0224, FSR 0236, FSR 0238, NGC 6910, RSL-04, RSL-05, RSL-06, HSC 625, OC-123, OC-128, Bica 1 and Bica 2 suggests that these OCs would be related to the Cyg OB2 association. RSL-02 ≡ HSC 630, located at 1346 pc, has similar values of mean proper motion and distance to those of the Left over-density named by Orellana *et al.* (2021) [9], suggesting that both objects would be related.

We also identified the members for each of the clusters found in the region. When comparing our results with those present in the literature, we find significant differences especially with those reported by Hunt & Reffert (2023) [19]. Our analysis demonstrates that these differences are due to the presence of false positives in their results which arise from neglecting the uncertainties in parallaxes. For this reason, we adopt parallaxes with a fractional error $f = \frac{\sigma_{\varpi}}{\varpi} \leq 0.20$ in order to eliminate spurious data and ensure the reliability of our results (criterion v). The low percentage of common members, as shown in **Figure 4** and **Table 4**, reflects the influence of the selection criteria adopted. Having more accurate membership lists enables a better characterization of clusters.

Through the analysis of *Gaia* and NIR 2MASS photometric data, using PARSEC isochrone models, we study the physical parameters of the four new open clusters detected, IRAS-20306+4005, HSC 630, and four OCs within the Cyg OB2 core. The age range for these clusters would be between 4 and 26 Myr, and the visual absorption ranges from 1.3 to 6.3 mag.

Acknowledgements

We thank E. Giorgi and R. Vallverdú for many useful comments which improved this paper. This work has made use of data from the European Space Agency (ESA) mission *Gaia* (https://www.cosmos.esa.int/gaia), processed by the *Gaia* Data Processing and Analysis Consortium (DPAC, https://www.cosmos.esa.int/web/gaia/dpac/consortium). Funding for the DPAC has been provided by national institutions, in particular the institutions participating in the *Gaia* Multilateral Agreement.

This research has made use of "Aladin sky atlas" developed at CDS, Strasbourg Observatory, France [49].

This research has made use of the APASS database, located at the AAVSO web site. Funding for APASS has been provided by the Robert Martin Ayers Sciences Fund.

This work was supported by Consejo Nacional de Investigaciones Científicas y Técnicas (CONICET), Argentina, under grants PIP 0507 and by Universidad Nacional de La Plata (UNLP), Argentina, under grants no. 11/G172 and PPID/G005.

Conflicts of Interest

The authors declare no conflicts of interest regarding the publication of this paper.

References

[1] Dias, W.S., Alessi, B.S., Moitinho, A. and Lépine, J.R.D. (2002) New Catalogue of Optically Visible Open Clusters and Candidates. *Astronomy & Astrophysics*, **389**, 871-873. https://doi.org/10.1051/0004-6361:20020668

[2] Kharchenko, N.V., Piskunov, A.E., Schilbach, E., Röser, S. and Scholz, R.-D. (2013) Global Survey of Star Clusters in the Milky Way. *Astronomy & Astrophysics*, **558**, A53. https://doi.org/10.1051/0004-6361/201322302

[3] Luri, X., Brown, A.G.A., Sarro, L.M., Arenou, F., Bailer-Jones, C.A.L., Castro-Ginard, A., *et al.* (2018) *Gaia* Data Release 2: Summary of the Contents and Survey Properties. *Astronomy & Astrophysics*, **616**, A1.

[4] Cantat-Gaudin, T., Jordi, C., Vallenari, A., Bragaglia, A., Balaguer-Núñez, L., Soubiran, C., *et al.* (2018) A *Gaia* DR2 View of the Open Cluster Population in the Milky Way. *Astronomy & Astrophysics*, **618**, A93. https://doi.org/10.1051/0004-6361/201833476

[5] Cantat-Gaudin, T., Anders, F., Castro-Ginard, A., Jordi, C., Romero-Gómez, M., Soubiran, C., *et al.* (2020) Painting a Portrait of the Galactic Disc with Its Stellar Clusters. *Astronomy & Astrophysics*, **640**, A1. https://doi.org/10.1051/0004-6361/202038192

[6] Dias, W.S., Monteiro, H., Moitinho, A., Lépine, J.R.D., Carraro, G., Paunzen, E., *et al.* (2021) Updated Parameters of 1743 Open Clusters Based on *Gaia* DR2. *Monthly Notices of the Royal Astronomical Society*, **504**, 356-371. https://doi.org/10.1093/mnras/stab770

[7] Sim, G., Lee, S., Ann, H. and Kim, S. (2019) 207 New Open Star Clusters within 1 Kpc from *Gaia* Data Release 2. *Journal of the Korean Astronomical Society*, **52**, 145-158.

[8] Casado, J. (2021) New Open Clusters Found by Manual Mining of Data Based on *Gaia* DR2. *Research in Astronomy and Astrophysics*, **21**, Article 117. https://doi.org/10.1088/1674-4527/21/5/117

[9] Orellana, R.B., De Biasi, M.S. and Paíz, L.G. (2021) New Members of Cygnus OB2 from *Gaia* DR2. *Monthly Notices of the Royal Astronomical Society*, **502**, 6080-6093. https://doi.org/10.1093/mnras/stab457

[10] Liu, L. and Pang, X. (2019) A Catalog of Newly Identified Star Clusters in *Gaia* DR2. *The Astrophysical Journal Supplement Series*, **245**, Article 32. https://doi.org/10.3847/1538-4365/ab530a

[11] Castro-Ginard, A., Jordi, C., Luri, X., Cantat-Gaudin, T. and Balaguer-Núñez, L. (2019) Hunting for Open Clusters in *Gaia* DR2: The Galactic Anticentre. *Astronomy & Astrophysics*, **627**, A35. https://doi.org/10.1051/0004-6361/201935531

[12] Castro-Ginard, A., Jordi, C., Luri, X., Álvarez Cid-Fuentes, J., Casamiquela, L., Anders, F., *et al.* (2020) Hunting for Open Clusters in *Gaia* DR2: 582 New Open Clusters in the Galactic Disc. *Astronomy & Astrophysics*, **635**, A45. https://doi.org/10.1051/0004-6361/201937386

[13] He, Z., Xu, Y., Hao, C., Wu, Z. and Li, J. (2021) A Catalogue of 74 New Open Clusters Found in *Gaia* Data-Release 2. *Research in Astronomy and Astrophysics*, **21**, Article 093. https://doi.org/10.1088/1674-4527/21/4/93

[14] Vallenari, A., Brown, A.G.A., Prusti, T., de Bruijne, J.H.J., Arenou, F., Babusiaux, C., *et al.* (2023) *Gaia* Data Release 3: Summary of the Content and Survey Properties. *Astronomy & Astrophysics*, **674**, A1. https://doi.org/10.1051/0004-6361/202243940

[15] *Gaia* Collaboration (2021) *Gaia* Early Data Release 3. Summary of the Contents and

Survey Properties. *Astronomy and Astrophysics*, **649**, A1.

[16] Li, Z., Deng, Y., Chi, H., Chen, J., Liu, X., Yan, C., *et al.* (2022) LISC Catalog of Star Clusters. I. Galactic Disk Clusters in *Gaia* EDR3. *The Astrophysical Journal Supplement Series*, **259**, Article 19. https://doi.org/10.3847/1538-4365/ac3c49

[17] Hao, C.J., Xu, Y., Wu, Z.Y., Lin, Z.H., Liu, D.J. and Li, Y.J. (2022) Newly Detected Open Clusters in the Galactic Disk Using *Gaia* EDR3. *Astronomy & Astrophysics*, **660**, A4. https://doi.org/10.1051/0004-6361/202243091

[18] Castro-Ginard, A., Jordi, C., Luri, X., Cantat-Gaudin, T., Carrasco, J.M., Casamiquela, L., *et al.* (2022) Hunting for Open Clusters in *Gaia* EDR3: 628 New Open Clusters Found with OCfinder. *Astronomy & Astrophysics*, **661**, A118. https://doi.org/10.1051/0004-6361/202142568

[19] Hunt, E.L. and Reffert, S. (2023) Improving the Open Cluster Census. II. An All-Sky Cluster Catalogue with *Gaia* DR3 *Astronomy & Astrophysics*, **673**, A114. https://doi.org/10.1051/0004-6361/202346285

[20] Lindegren, L., Bastian, U., Biermann, M., Bombrun, A., de Torres, A., Gerlach, E., *et al.* (2021) *Gaia* Early Data Release 3. Parallax Bias Versus Magnitude, Colour, and Position *Astronomy & Astrophysics*, **649**, A4. https://doi.org/10.1051/0004-6361/202039653

[21] Skrutskie, M.F., Cutri, R.M., Stiening, R., Weinberg, M.D., Schneider, S., Carpenter, J.M., *et al.* (2006) The Two Micron All Sky Survey (2MASS). *The Astronomical Journal*, **131**, 1163-1183. https://doi.org/10.1086/498708

[22] Fabricius, C., Luri, X., Arenou, F., Babusiaux, C., Helmi, A., Muraveva, T., *et al.* (2021) *Gaia* Early Data Release 3. Catalogue Validation. *Astronomy & Astrophysics*, **649**, A5. https://doi.org/10.1051/0004-6361/202039834

[23] Campello, R.J.G.B., Moulavi, D. and Sander, J. (2013) Density-Based Clustering Based on Hierarchical Density Estimates. In: Pei, J., Tseng, V.S., Cao, L., Motoda, H. and Xu, G., Eds., *Lecture Notes in Computer Science*, Springer, 160-172. https://doi.org/10.1007/978-3-642-37456-2_14

[24] Alfonso, J., García-Varela, A. and Vieira, K. (2024) Exploring Galactic Open Clusters with *Gaia*. I. An Examination in the First Kiloparsec. *Astronomy & Astrophysics*, **689**, A18. https://doi.org/10.1051/0004-6361/202450901

[25] Hunt, E.L. and Reffert, S. (2021) Improving the Open Cluster Census. I. Comparison of Clustering Algorithms Applied to *Gaia* DR2 Data. *Astronomy & Astrophysics*, **646**, A104. https://doi.org/10.1051/0004-6361/202039341

[26] Sampedro, L. and Alfaro, E.J. (2016) Stellar Open Clusters' Membership Probabilities: An *N*-Dimensional Geometrical Approach. *Monthly Notices of the Royal Astronomical Society*, **457**, 3949-3962. https://doi.org/10.1093/mnras/stw243

[27] Negueruela, I., Marco, A., Israel, G.L. and Bernabeu, G. (2007) Pre-Main-Sequence Stars in the Young Open Cluster NGC 1893. II. Evidence for Triggered Massive Star formation. *Astronomy & Astrophysics*, **471**, 485-497. https://doi.org/10.1051/0004-6361:20066654

[28] Borissova, J., Georgiev, L., Hanson, M.M., Clarke, J.R.A., Kurtev, R., Ivanov, V.D., *et al.* (2012) Obscured Clusters. IV. The Most Massive Stars in [DBS2003] 179. *Astronomy & Astrophysics*, **546**, A110. https://doi.org/10.1051/0004-6361/201118348

[29] Messineo, M., Menten, K.M., Churchwell, E. and Habing, H. (2011) Near- and Mid-Infrared Colors of Evolved Stars in the Galactic Plane. The $Q1$ and $Q2$ Parameters. *Astronomy & Astrophysics*, **537**, A10. https://doi.org/10.1051/0004-6361/201117772

[30] Green, G.M., Schlafly, E., Zucker, C., Speagle, J.S. and Finkbeiner, D. (2019) A 3D

Dust Map Based on *Gaia*, Pan-STARRS 1, and 2MASS. *The Astrophysical Journal*, **887**, Article 93. https://doi.org/10.3847/1538-4357/ab5362

[31] Wright, N.J., Drew, J.E. and Mohr-Smith, M. (2015) The Massive Star Population of Cygnus OB2. *Monthly Notices of the Royal Astronomical Society*, **449**, 741-760. https://doi.org/10.1093/mnras/stv323

[32] Bressan, A., Marigo, P., Girardi, L., Salasnich, B., Dal Cero, C., Rubele, S., *et al.* (2012) PARSEC: Stellar Tracks and Isochrones with the Padova and Trieste Stellar Evolution Code. *Monthly Notices of the Royal Astronomical Society*, **427**, 127-145. https://doi.org/10.1111/j.1365-2966.2012.21948.x

[33] Fu, X., Bragaglia, A., Liu, C., Zhang, H., Xu, Y., Wang, K., *et al.* (2022) LAMOST Meets *Gaia*: The Galactic Open Clusters. *Astronomy & Astrophysics*, **668**, A4. https://doi.org/10.1051/0004-6361/202243590

[34] Qin, S., Zhong, J., Tang, T. and Chen, L. (2023) Hunting for Neighboring Open Clusters with *Gaia* DR3: 101 New Open Clusters within 500 Pc. *The Astrophysical Journal Supplement Series*, **265**, Article 12. https://doi.org/10.3847/1538-4365/acadd6

[35] Bailer-Jones, C.A.L. (2015) Estimating Distances from Parallaxes. *Publications of the Astronomical Society of the Pacific*, **127**, 994-1009. https://doi.org/10.1086/683116

[36] Luri, X., Brown, A.G.A., Sarro, L.M., Arenou, F., Bailer-Jones, C.A.L., Castro-Ginard, A., *et al.* (2018) *Gaia* Data Release 2. Using *Gaia* Parallaxes. *Astronomy & Astrophysics*, **616**, A9. https://doi.org/10.1051/0004-6361/201832964

[37] Bailer-Jones, C.A.L., Rybizki, J., Fouesneau, M., Demleitner, M. and Andrae, R. (2021) Estimating Distances from Parallaxes. V. Geometric and Photogeometric Distances to 1.47 Billion Stars in *Gaia* Early Data Release 3. *The Astronomical Journal*, **161**, Article 147. https://doi.org/10.3847/1538-3881/abd806

[38] Dias, W.S., Alessi, B.S., Moitinho, A. and Lepine, J.R.D. (2014) New Catalogue of Optically Visible Open Clusters and Candidates. *Astronomy & Astrophysics* (*A&A*), **389**, 871-873. https://www.aanda.org/articles/aa/abs/2002/27/aa2476/aa2476.html

[39] Belokurov, V., Penoyre, Z., Oh, S., Iorio, G., Hodgkin, S., Evans, N.W., *et al.* (2020) Unresolved Stellar Companions with *Gaia* DR2 Astrometry. *Monthly Notices of the Royal Astronomical Society*, **496**, 1922-1940. https://doi.org/10.1093/mnras/staa1522

[40] Lindegren, L. (2022) Expected Astrometric Properties of Binaries in (E)DR3. https://dms.cosmos.esa.int/COSMOS/doc_fetch.php?id=1566327

[41] Castro-Ginard, A., Penoyre, Z., Casey, A.R., Brown, A.G.A., Belokurov, V., Cantat-Gaudin, T., *et al.* (2024) *Gaia* DR3 Detectability of Unresolved Binary Systems. *Astronomy & Astrophysics*, **688**, A1. https://doi.org/10.1051/0004-6361/202450172

[42] Rivera-Gálvez, S., Román-Zúñiga, C.G., Jiménez-Bailón, E., Ybarra, J.E., Alves, J.F. and Lada, E.A. (2015) The Young Stellar Population of the Cygnus-X DR15 Region. *The Astronomical Journal*, **150**, Article 191. https://doi.org/10.1088/0004-6256/150/6/191

[43] Chen, X., Wang, S., Deng, L., de Grijs, R., Yang, M. and Tian, H. (2020) The Zwicky Transient Facility Catalog of Periodic Variable Stars. *The Astrophysical Journal Supplement Series*, **249**, Article 18. https://doi.org/10.3847/1538-4365/ab9cae

[44] Kuhn, M.A., de Souza, R.S., Krone-Martins, A., Castro-Ginard, A., Ishida, E.E.O., Povich, M.S., *et al.* (2021) SPICY: The Spitzer/IRAC Candidate YSO Catalog for the Inner Galactic Midplane. *The Astrophysical Journal Supplement Series*, **254**, Article 33. https://doi.org/10.3847/1538-4365/abe465

[45] Rauw, G. (2011) A Multi-Epoch *XMM-Newton* Campaign on the Core of the Massive

Cygnus OB2 Association. *Astronomy & Astrophysics*, **536**, A31. https://doi.org/10.1051/0004-6361/201117648

[46] Bhattacharyya, S., Mathew, B., Banerjee, G., Anusha, R., Paul, K.T. and Kartha, S.S. (2021) Identification of Emission-Line Stars in Transition Phase from Pre-Main Sequence to Main Sequence. *Monthly Notices of the Royal Astronomical Society*, **507**, 3660-3671. https://doi.org/10.1093/mnras/stab2385

[47] Bica, E., Bonatto, C. and Dutra, C.M. (2003) Does Cyg OB2 Harbour Any Open Cluster? *Astronomy & Astrophysics*, **405**, 991-998. https://doi.org/10.1051/0004-6361:20030700

[48] Maíz Apellániz, J., Crespo Bellido, P., Barbá, R.H., Fernández Aranda, R. and Sota, A. (2020) The Villafranca Catalog of Galactic OB Groups. I. Systems with O2-O3.5 Stars. *Astronomy & Astrophysics*, **643**, A138. https://doi.org/10.1051/0004-6361/202038228

[49] Bonnarel, F., Fernique, P., Bienaymé, O., Egret, D., Genova, F., Louys, M., *et al.* (2000) The ALADIN Interactive Sky Atlas. *Astronomy and Astrophysics Supplement Series*, **143**, 33-40. https://doi.org/10.1051/aas:2000331